Water Oxidation Hot Paper

How to cite: *Angew. Chem. Int. Ed.* **2021**, *60*, 13463–13469
International Edition: doi.org/10.1002/anie.202103157
German Edition: doi.org/10.1002/ange.202103157

Ligand Controls the Activity of Light-Driven Water Oxidation Catalyzed by Nickel(II) Porphyrin Complexes in Neutral Homogeneous Aqueous Solutions

*Chengyu Liu, Daan van den Bos, Barthold den Hartog, Dennis van der Meij, Ashok Ramakrishnan, and Sylvestre Bonnet**

Abstract: *Finding photostable, first-row transition metal-based molecular systems for photocatalytic water oxidation is a step towards sustainable solar fuel production. Herein, we discovered that nickel(II) hydrophilic porphyrins are molecular catalysts for photocatalytic water oxidation in neutral to acidic aqueous solutions using $[Ru(bpy)_3]^{2+}$ as photosensitizer and $[S_2O_8]^{2-}$ as sacrificial electron acceptor. Electron-poorer Ni-porphyrins bearing 8 fluorine or 4 methylpyridinium substituents as electron-poorer porphyrins afforded 6-fold higher turnover frequencies (TOFs; ca. 0.65 min^{-1}) than electron-richer analogues. However, the electron-poorest Ni-porphyrin bearing 16 fluorine substituents was photocatalytically inactive under such conditions, because the potential at which catalytic O_2 evolution starts was too high (+1.23 V vs. NHE) to be driven by the photochemically generated $[Ru(bpy)_3]^{3+}$. Critically, these Ni-porphyrin catalysts showed excellent stability in photocatalytic conditions, as a second photocatalytic run replenished with a new dose of photosensitizer, afforded only 1–3 % less O_2 than during the first photocatalytic run.*

Introduction

Photochemical water oxidation plays a critical role for artificial photosynthesis and solar fuel production, as water represents the most sustainable source of electrons for CO_2 and proton reduction.[1–10] In particular, molecular water oxidation catalysts capable of generating O_2 in homogeneous conditions and under the action of light, have generated great attention because they form the basis for integrated supramolecular solar fuel-generated devices. In principle, such complexes offer fascinating possibilities of varying the ligands with atomic precision, which allows for fine-tuning the coordination sphere and electron density of the metal-based catalyst, to optimize catalytic efficacy.[11,12] However, many molecular catalysts initially thought to act as molecules in photocatalytic water oxidation systems, were later shown to decompose, in the harsh conditions of photocatalytic water oxidation, into metal oxides, which are themselves catalytically active in the oxygen evolution reaction (OER). It is hence critical, before claiming that a molecular catalyst is catalytically active as a molecule, to demonstrate its stability in photocatalytic conditions.

Although molecular catalysts based on ruthenium or iridium still offer the highest stabilities and activities for photocatalytic water oxidation to date,[13–16] those made of first-row transition metals such as V,[17,18] Mn,[18,19] Fe,[20,21] Co,[22–35] and Cu[36,37] have received increased attention recently because of their lower cost and greater abundance on Earth. However, most of them are only active in alkaline environment, which is sub-optimal for photocatalytic solar fuel generation systems combining water oxidation and either proton or CO_2 reduction, which typically require more neutral or even acidic (CO_2-saturated) conditions. Nickel is earth-abundant as well, and a few Ni^{II} complexes have been recently proposed as molecular catalysts for electrocatalytic OER,[38–41] where they showed high activities in pH-neutral aqueous solutions. However, molecular nickel-based water oxidation catalysts remain rare in artificial photosynthesis.[11] There is to our knowledge no demonstration of the use of Ni^{II} complexes for the OER in photocatalytic conditions, with the exception of a report from Chen et al,[42] showing photocatalytic water oxidation with Ni-based precursor complexes that clearly serve as pre-catalysts that become active only after decomposition into Ni oxide.

Herein, we report a series of four tetraanionic Ni^{II}-porphyrin complexes bearing either electron-donating (Ni-OMe, Ni-Me) or electron-withdrawing (Ni-F8, Ni-F16) substituents (Figure 1). These catalysts were found active for the photocatalytic OER in homogeneous aqueous solutions in presence of $[Ru(bpy)_3]Cl_2$ as photosensitizer (PS), $Na_2S_2O_8$ as sacrificial electron acceptor (EA), blue light (450 nm), and at neutral to acidic pH. The four substitution patterns, from electron-rich Ni-OMe to the electron poor Ni-F16, were designed based on the simplified photocatalytic mechanism for water oxidation shown in Figure 2. In Step 1, the photosensitizer PS absorb a photon and is excited to an excited state that transfers an electron to $[S_2O_8]^{2-}$ to afford PS^+ ($[Ru^{III}(bpy)_3]^{3+}$), $[SO_4]^{2-}$, and a $[SO_4]^{\bullet-}$ radical that further oxidizes a second equivalent of PS to PS^+ (Figure S3).[43,44] In Step 2, PS^+ oxidizes with an electron-transfer

[*] C. Liu, D. van den Bos, B. den Hartog, D. van der Meij, A. Ramakrishnan, Prof. S. Bonnet
Leiden Institute of Chemistry, Leiden University
Einsteinweg 55, PO Box 9502, 2333CC Leiden (The Netherlands)
E-mail: Bonnet@chem.leidenuniv.nl
Supporting information and the ORCID identification number(s) for the author(s) of this article can be found under: https://doi.org/10.1002/anie.202103157.

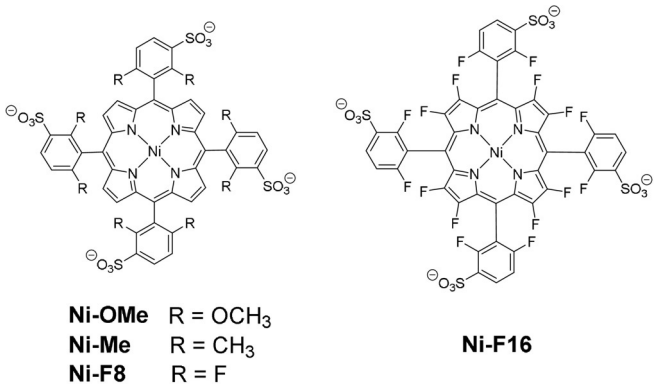

Figure 1. Chemical structures of water soluble Ni^{II}-porphyrin complexes used in this work, isolated with Na^+ counter ions.

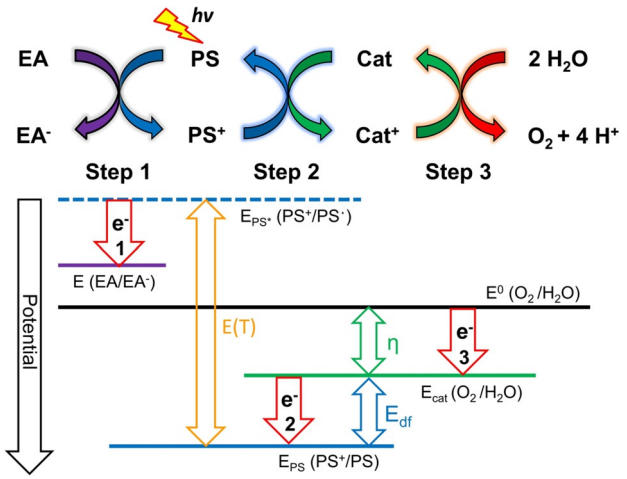

Figure 2. Simplified photocatalytic mechanism and energy scheme of a three-component molecular homogeneous photocatalytic water oxidation system. EA: sacrificial electron acceptor; PS: photosensitizer; Cat: water oxidation catalyst; E(T): triplet exited state energy; η: overpotential of Cat; E_{df}: driving force of the electron transfer from the catalyst to the oxidized photosensitizer.

driving force E_{df} the water oxidation catalyst (Cat) into Cat^+, which, after several repetitions of the same process, affords higher oxidation states of the catalyst capable to oxidize water catalytically, which corresponds to Step 3. The driving force for this last step, usually referred to as the overpotential η, corresponds to the potential at which the catalyst turns over significantly, to afford O_2 and 4 protons. The exceptional stability of the nickel(II) catalysts presented here enabled us to study the influence of the electron-donating and -withdrawing substituents of the nickel complexes on its redox properties,[45] on the interplay between E_{df} and η, and to relate these redox properties to the overall performances of the photocatalytic system (Figure 2). Since the charge of the catalyst may affect the electron transfer rate of Step 2,[46] two known positively charged Ni^{II}-porphyrin complexes Ni-MPy and Ni-TMA were included in this study as well, the chemical structures of which are shown in Figure S4. By interrogating the mechanism shown in Figure 2, we established design principle on how η and E_{df} should be balanced to develop molecular catalysts that maximize the performances of photocatalytic water oxidation.

Results and Discussion

The tetrasulfonated porphyrin ligands H2-Me, H2-F8, and H2-F16 were synthesized according to reported procedures,[47–51] while H2-OMe was synthesized by sulfonation using chlorosulfonic acid in anhydrous CH_2Cl_2 at room temperature. All four Ni^{II} complexes were obtained by refluxing the free-base tetrasulfonatoporphyrin ligands with Ni^{II} acetate in Milli-Q water for 12 h under N_2. Na^+-loaded ion exchange resin was used to enforce Na^+ counter ions, and the complexes were finally purified by size-exclusion chromatography in order to remove the excess inorganic salts. The analytical purity of H2-OMe, Ni-OMe, Ni-Me, Ni-F8 and Ni-F16, was established by NMR (Figure S5–12), high-resolution MS, and elemental analysis.

In photocatalytic conditions using $[Ru(bpy)_3]Cl_2$ as the PS, $Na_2S_2O_8$ as EA, and blue light irradiation (450 nm), most molecular nickel catalysts tested in this study were found to produce O_2, but the oxygen evolution performances of the electron-poor nickel complexes Ni-F8 and Ni-MPy were found significantly better than that of the electron-richer complexes Ni-OMe and Ni-Me (Figure 3). Quite surprisingly, the electron-poorest complex, Ni-F16, showed no photocatalytic activity at all in these conditions, while nickel(II) acetate (Ni-Ac), used as control, showed very low photocatalytic activity. This last result suggests either that the homogeneous $[Ni(OH_2)_6]^{2+}$ ions, or the nickel oxide nanoparticles deriving from decomposition of these ions in photocatalytic conditions, were not active.

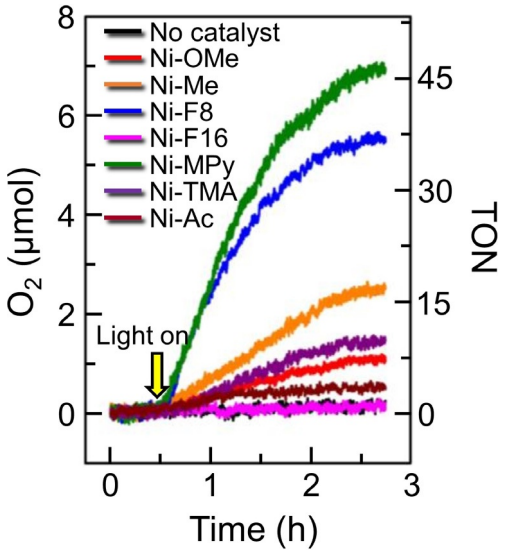

Figure 3. Dioxygen evolution during water photocatalytic oxidation in presence of 0.05 mM catalyst Ni-OMe, Ni-Me, Ni-F8, Ni-F16, Ni-MPy, Ni-TMA, and Ni^{II} acetate (Ni-Ac), using 0.67 mM $[Ru(bpy)_3]Cl_2$ as photosensitizer, 50 mM $Na_2S_2O_8$ in 0.1 M pH 7.0 sodium phosphate buffer, and LED lamp (450 nm, 15.8 mW) for irradiation. T = 298 K.

Considering the interesting photocatalytic activity of some of these Ni-porphyrin complexes, it was essential to test whether these compounds were catalytically active as homogeneous molecular species, or simply pre-catalysts decomposing into nickel oxide nanoparticles, which have been shown repeatedly to catalyze the OER.[42] Several experiments were realized to investigate this question. First, phosphate-buffered solutions of each Ni-porphyrin complex at pH 7.0 was irradiated with blue light (450 nm, 15.8 mW) and their UV-vis spectrum followed in time during 3 h. The spectra did not change during irradiation (Figure S13–18), showing the intrinsic photostability of these molecules in absence of electron acceptor and photosensitizer. Second, dynamic light scattering (DLS) analysis was performed for full photocatalytic mixtures containing, next to PS and $Na_2S_2O_8$, either a Ni-porphyrin complexes or $NiOAc_2$. These measurements concluded that when photocatalysis was realized at an initial neutral pH (7.0) and run for 0.5, 1.0, 1.5, 2.0 h, no NiO_x nanoparticles were formed. As a positive control, photocatalytic experiments performed using $NiOAc_2$ as the catalyst but realized at an initial basic pH (8.5), did show significant NiO_x nanoparticles formation (Figure 4a). Hence, in the photocatalytic conditions of Figure 3 none of the Ni^{II} porphyrin catalysts decomposed into nickel oxide nanoparticles. In a third experiment, after a first 2.75 h photocatalytic run with Ni-F8 for example, the photocatalytic mixture was clearly deactivated and did not produce O_2 anymore; the final pH was significantly reduced (typically $\approx$2.8) and the TON was 36.5. When such a solution was neutralized by addition of NaOH, re-filled with a new batch of photosensitizer and of $Na_2S_2O_8$, and irradiated further in the same conditions, O_2 production resumed with very similar rates as during the first photocatalytic run (Figure 4b). After 2.25 h light irradiation the final O_2 evolution for Ni-MPy was only 7% lower compared to the first run, and for Ni-OMe, Ni-Me, Ni-F8, and Ni-TMA the loss was only 1–3% (see Figure 4b for Ni-F8, and Figure S19 for Ni-OMe, Ni-Me, Ni-MPy and Ni-TMA).

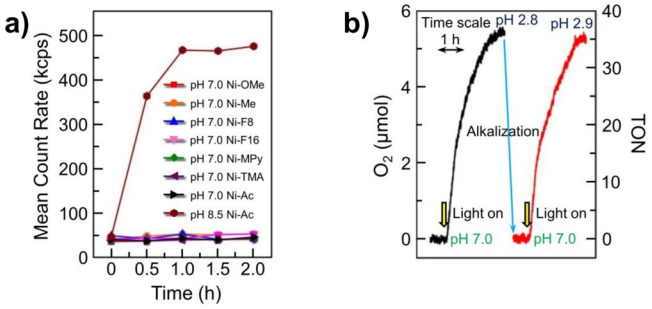

Figure 4. a) Dynamic light scattering analysis after various times of photocatalytic water oxidation with different catalysts. Conditions: 50 mM $Na_2S_2O_8$, 0.67 mM $[Ru(bpy)_3]Cl_2$ and 0.05 mM water oxidation catalyst Ni-OMe, Ni-Me, Ni-F8, Ni-F16, Ni-MPy, Ni-TMA, or Ni^{II} acetate (Ni-Ac) in 0.1 M pH 7.0 phosphate buffer, and 50 mM $Na_2S_2O_8$, 0.67 mM $[Ru(bpy)_3]Cl_2$ and 0.05 mM Ni-Ac in 0.1 M pH 8.5 phosphate buffer. Conditions: blue light (450 nm, 15.8 mW), $T = 298$ K. b) Repetitive photocatalytic water oxidation using a homogeneous mixture containing 0.05 mM Ni-F8 with 0.67 mM $[Ru(bpy)_3]Cl_2$ and 50 mM $Na_2S_2O_8$ in 0.1 M sodium phosphate buffer (initial pH 7.0), using blue light (450 nm, 15.8 mW), $T = 298$ K. Between the two irradiation experiments, neutralization was realized by adding NaOH solid by checking pH, 0.67 mM fresh $[Ru(bpy)_3]Cl_2$ and 50 mM $Na_2S_2O_8$ as solids were added.

As a side note, the pH change during Ni-catalyzed photocatalytic water oxidation is remarkable, but it was reported before.[13] Actually, the pH change from 7.0 to 2.8 was also observed when irradiating, in the same conditions as above, a solution containing the Ru photosensitizer and $Na_2S_2O_8$ but deprived of Ni catalyst (Figure S20). The pH change in photocatalytic conditions can hence essentially be explained by photosensitizer decomposition. Ghosh et al. reported that formic acid may form by oxidation of the bipyridine ligands when $[Ru(bpy)_3]^{3+}$ is dissolved in aqueous solutions.[52] We indeed found both acetic and formic acid by ^1H NMR analysis of a D_2O solution containing 0.67 mM $[Ru(bpy)_3]Cl_2$ and 50 mM $Na_2S_2O_8$ irradiated for 2.25 h with blue light (450 nm, 15.8 mW, Figure S21), which suggested that the reasons causing the pH decrease was at least partly due to the formation of small organic acids deriving from oxidation of the bipyridine ligands of the photosensitizer. It was repeatedly reported that $[Ru(bpy)_3]Cl_2$ was not photostable in aqueous photocatalytic conditions.[43] Such instability obviously explains the limited TON observed in Figure 3; one should note, however, that another possible consequence of a lowered pH could be catalyst inactivation, because for some WOC the onset oxidation potential of the catalyst may shift upwards at lower pH.[13] Here the CV and DPV of Ni-F8 at pH 2.8 (Figure S22) showed that OER indeed started at a higher potential at pH 2.8 (+1.24 V vs. NHE) than at pH 7.0 (+1.12 V vs.NHE), but that the catalyst was still active for the OER, even in such acidic conditions.

In presence of all four components of the photocatalytic system (Ni-F8), a second photocatalytic run realized after adding fresh PS showed good activity (Figure S23). This experiment suggested that photosensitizer decomposition was the main reason for the loss of photocatalytic activity, while the Ni-F8 catalyst could indeed cope with the lower pH 2.8 obtained in the end of the first photocatalytic run. In addition, the second photocatalytic run was limited by the low concentration of $Na_2S_2O_8$ remaining in the solution after the first photocatalytic run. Indeed, adding only a new batch of fresh PS to the deactivated solution, did not reactivate the system, while after adding another batch of fresh $Na_2S_2O_8$ as well, the system evolved O_2 a third time, demonstrating the good stability of the catalyst. In this photocatalytic system, the depletion of photosensitizer and electron acceptor were the main reasons that limited the turnover numbers. Overall, this series of Ni-porphyrin complexes showed great photostability not only in absence of photosensitizer and electron acceptor, but also in full photocatalytic conditions. Such stability comes in great contrast with $[Ru(bda)(isoq)_2]$ for example (H_2bda = 2,2′-bipyridine-6,6′-dicarboxylic acid; isoq = isoquinoline), which decomposed in parallel to the $[Ru(bpy)_3]^{2+}$ photosensitizer.[53] These results also demonstrate that the catalytic activity of the Ni-porphyrin complexes is indeed due to the presence of molecular species dissolved in a homogeneous solution, rather than nickel oxide nanoparticles.

As photocatalysis seemed to be run by molecular species, it should be possible to correlate the molecular formulae of

these complexes and the electron density of their metal center, to their (photo)catalytic activities. Their redox properties were hence determined by a combination of cyclic voltammetry (CV) and differential pulse voltammetry (DPV) in 0.1 M pH 7.0 phosphate buffer using a glassy-carbon (GC) electrode (Figure S24). According to CV, the electron-richer complexes Ni-OMe and Ni-Me showed slower kinetics for the electrocatalytic OER than the electron-poorer Ni-F8 and Ni-F16, as demonstrated by their lower catalytic current density compared with the blanks. Second, while Ni-OMe showed a single DPV waves, all other complexes showed two of them, with electron-poorer Ni-porphyrin complexes having higher DPV oxidation wave potentials. The second DPV wave is usually proposed as the potential at which electrocatalytic O_2 production actually starts.[1] To check this hypothesis, a controlled potential electrolysis (CPE) experiment was realized in a pH 7.0 phosphate-buffered solution using a system equipped with a Clark electrode for O_2 quantification. With Ni-F8 (2 mM), a CPE experiment run at the potential of the first DPV wave (+0.98 V vs. NHE) did not evolve any oxygen. However, at the potential of the second DPV wave (+1.12 V vs. NHE) the solution indeed produced O_2 significantly and the current was stable (Figure S25a,b). This observation suggested that the first oxidation of Ni-F8 formed oxidized species Ni^{II}-por$^{\bullet+}$ or Ni^{III}-por that is not able to catalyze water oxidation and hence can be reduced back to Ni^{II}-por, thus explaining the quasi-reversible redox process at $E_{1/2}$ = +0.98 V vs. NHE. Upon a second electron transfer at the second DPV wave potential, a catalytically active species was formed, which may be either Ni^{IV}-por or Ni^{III}-por$^{\bullet+}$.[1,39] When the GC electrode used in a first electrolytic run, was rinsed by Milli-Q water and used in a second electrocatalytic run using fresh buffer, no OER activity was observed (Figure S25c). In addition, the UV-vis spectra of the solution before and after CPE showed no difference (Figure S25d). Finally, the faradaic yield of the CPE system was 95 ± 5%. Overall, Ni-F8 was hence stable in electrocatalytic conditions, and the oxygen evolution from the CPE system was actually catalyzed by the molecular Ni-F8 complex, at the potential of the second DPV wave.

Ni-F16 behaved quite differently. This electron-poorer complex had, as expected from its higher number of electron-withdrawing substituents, higher DPV oxidation wave potentials (+1.23 and +1.42 V vs. NHE) compared to Ni-F8. However, in a 30 min CPE experiment, a 2 mM Ni-F16 solution electrocatalytically catalyzed the OER already at the first DVP wave potential (+1.23 V vs. NHE, see Figure S26) with a high Faradic yield (83 ± 3%) showing Ni-F16 could form an OER-active species upon 1-electron oxidation. We speculate that this electron-poor species may catalyze water oxidation via a binuclear radical coupling mechanism,[54,55] and that the second DPV wave, which corresponds to further 1-electron oxidation to Ni^{IV}-por or Ni^{III}-por$^{\bullet+}$, may catalyze water oxidation via a water nucleophilic attack, potentially with a higher energy barrier than the species formed by the first oxidation.[1,39] As a note, Ni-F16 was also stable during electrocatalytic OER according to UV-vis spectroscopy (Figure S26d). In photocatalytic conditions the photo-oxidized sensitizer PS^+ ($[Ru(bpy)_3]^{3+}$) has only a very low driving force E_{df} = 30 mV to trigger hole transfer from PS^+ (+1.26 V vs. NHE) to the catalyst (+1.23 V vs. NHE), and photocatalysis does not take place. Thus, photocatalytic water oxidation can be driven by Ni^{II}-porphyrin complexes provided the redox properties of the catalyst find an optimum: the complex should have a DPV oxidation wave potential that is high enough to be able to drive water oxidation (Step 3 in Figure 2) at appreciable overpotential η, but it should be low enough to keep an appreciable driving force E_{df} for the photosensitizer to drive Step 2. In this photocatalytic system, an electron transfer driving force E_{df} = 30 mV (with Ni-F16) was not high enough to drive photocatalysis, while E_{df} = 140 mV (with Ni-F8) was close to the optimum.

Interestingly, the relative sign of the charge of the molecular catalyst and of that of the photosensitizer, were found to play a limited role in the relation between redox potentials and photocatalytic rates. Replacing a tetraanionic Ni-porphyrin catalyst by a tetracationic Ni-porphyrin complexes such as Ni-MPy or Ni-TMA, did not introduce outliers in the trend discussed above (Figure 5). The second DPV oxidation wave potential of Ni-MPy is slightly higher (0.12 V) than that of Ni-F8, but still lower than the redox potential of the $[Ru(bpy)_3]^{3+}/[Ru(bpy)_3]^{2+}$ couple, and indeed a slightly higher TOF was found in photocatalytic conditions for this complex. On the other hand, the second DPV oxidation wave potential of Ni-TMA was lower than that of Ni-Me, and indeed a slightly lower TOF was found in photocatalysis. Hence it seems that in the series of nickel water oxidation catalysts Ni-OMe, Ni-Me, Ni-F8, Ni-F16, Ni-TMA and Ni-MPy, the electron-donating and -withdrawing nature of the porphyrin substituents is the main variable responsible for the evolution of the photocatalytic efficiency, while the charge of the complex plays a minor role. Overall, Ni-F8 and Ni-MPy were found the most active catalysts of this series of nickel complexes for photocatalytic OER. They offer the best compromise in terms of redox potential, i.e., an electro-

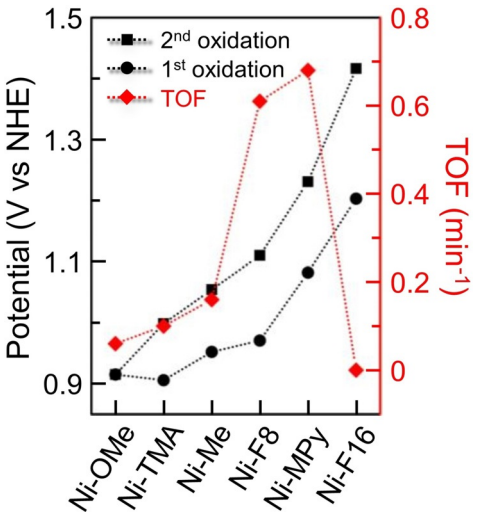

Figure 5. DPV oxidation wave potentials (left axis, first and second oxidation shown by circles and squares, respectively) for Ni-OMe, Ni-Me, Ni-F8, Ni-F16, Ni-MPy, Ni-TMA, and maximum TOF (right axis, red diamonds, min^{-1}) obtained in the photocatalytic water oxidation experiments described in Figure 3.

catalytically active DPV oxidation wave potential that is high enough to maximizes η and the rate of Step 3, but low enough for fast electron transfer in Step 2 to occur (Table S1).

As Ni-F8 ended up as an optimum for the series of new anionic complexes presented here, the mechanism of the photocatalytic OER in pH 7.0 phosphate buffer solution was further investigated. First, a first-order dependence of the O_2 evolution rate on catalyst concentration was observed using a fixed PS concentration of 0.67 mM (Figure 6a,b and Figure S27a), suggesting that the rate-determining step of the reaction involved one nickel center. Second, a first-order dependence of the O_2 evolution rate on PS concentration was found using a fixed Ni-F8 catalyst concentration of 50 μM (Figure 6c,d and Figure S27b), which showed that the rate-determining step of the photocatalytic system also involved one molecule of PS. Third, the TOF of the system was not significantly influenced by the photons flux when the light power was higher than 11 mW (Figure S28), showing that the photon density was in excess in such conditions, and that Step 1 did not limit the reaction rate. This last result was confirmed by an experiment showing that there was very limited change of the rate of O_2 production when the concentration of $Na_2S_2O_8$ was varied in the range 25–100 mM (Figure S29). Finally, when $[Ru(bpy)_3](ClO_4)_3$ was used as chemical oxidant, the maximum O_2 evolution rate of the catalytic system was found linearly dependent on both the concentrations of $[Ru(bpy)_3]^{3+}$ and that of the Ni-F8 catalyst (Figure S30), suggesting that the role of the sulfate radical liberated by 1-electron transfer from PS* to $S_2O_8^{2-}$, is minimal, i.e., that the photocatalytic O_2-evolution reaction is indeed driven by the photochemical generation of $[Ru(bpy)_3]^{3+}$. Altogether, these results strongly suggest that under such photocatalytic conditions, it is the electron transfer from the catalyst to the photo-oxidized photosensitizer PS^+, that is, Step 2 in Figure 1, that is the rate-determining step of the photocatalytic system. This result, which is reminiscent of a study published by our group using Sun's catalyst $[Ru(bda)(isoq)_2]$,[53] is not only important mechanistically speaking; it also demonstrates that the Ni-F8 catalyst is fast enough, at least for homogeneous photocatalytic water oxidation. Such a result is important because the catalytic activity of molecular water oxidation catalysts (hence the rate of Step 3) is often presented as the most important parameter to improve for achieving efficient production of solar fuels, while we see here that the rate of electron transfer can also be the bottleneck of the reaction. Assuming that only two photons are needed to produce four $[Ru(bpy)_3]^{3+}$ that can further evolve one O_2 molecule, the quantum yield for O_2 production using 0.05 mM Ni-F8 as the catalyst, 0.67 mM $[Ru(bpy)_3]Cl_2$ as PS, 50 mM $Na_2S_2O_8$ as EA and 15.8 mW of blue light (450 nm), was 0.29 ± 0.05 %. This modest value should be considered as strongly encouraging, as it is accompanied by an exceptional stability of the nickel catalysts in photocatalytic conditions, where it is the decomposition of the photosensitizer, and the depletion of peroxodisulfate, that limit the turnover number of the system.

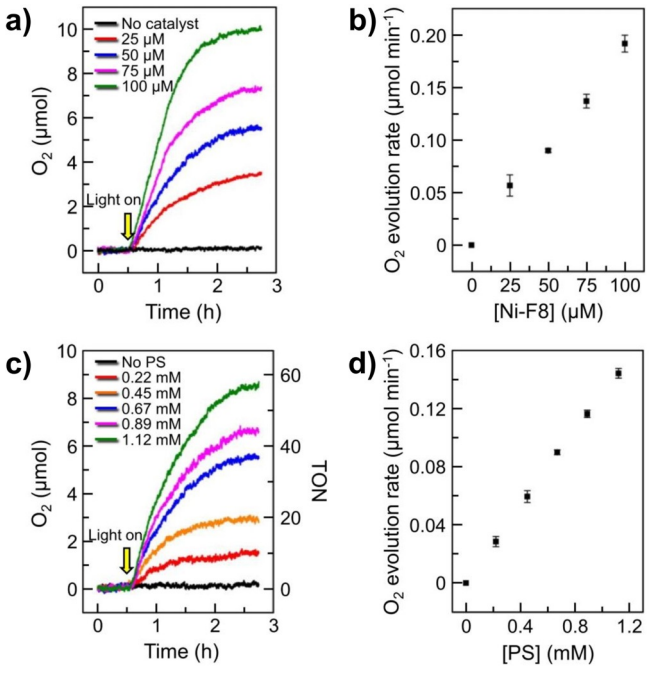

Figure 6. Photocatalytic oxygen evolution vs. irradiation time with a) different concentrations of Ni-F8 with 0.67 mM $[Ru(bpy)_3]Cl_2$ as photosensitizer, and c) different concentrations of PS with 50 μM Ni-F8 as WOC. b) and d) maximum O_2 evolution rate during photocatalytic O_2 evolution plotted as a function of b) the concentration of Ni-F8 and d) the concentration of $[Ru(bpy)_3]Cl_2$. Conditions: 50 mM $Na_2S_2O_8$ in 0.1 M sodium phosphate buffer (initial pH 7.0), blue light (450 nm, 15.8 mW), $T = 298$ K.

Conclusion

Here, a series of four anionic Ni-porphyrin complexes were prepared that showed promising catalytic properties for electrocatalytic and photocatalytic water oxidation in neutral to acidic phosphate-buffered homogeneous aqueous solutions. Electrochemical studies revealed that modifications of the tetrasulfonatoporphyrin ligand with more electron-withdrawing substituents increased the DPV oxidation wave potentials, which in turn strongly influenced the rate of the OER in photocatalytic conditions. A balance has to be found between increasing these oxidation potentials, which provide a higher driving force (η) for the nickel-catalyzed OER reaction itself, and lowering it, to keep the driving force for electron transfer from the catalyst to the oxidized photosensitizer PS^+ (E_{df}), high enough. Ni-F16, for example, was too electron-poor, which inactivated photocatalysis by blocking Step 2. A photosensitizer with a higher oxidation potential than $[Ru(bpy)_3]^{3+}/[Ru(bpy)_3]^{2+}$ may be able to alleviate this problem and unravel the otherwise excellent electrocatalytic OER properties of this complex. By contrast, Ni-F8 and Ni-MPy were found close to the optimum, at least for $[Ru(bpy)_3]^{2+}$ as photosensitizer, and offered excellent properties for the photocatalytic OER. Critically, these first-row transition metal complexes showed great stability both in photocatalytic and electrocatalytic conditions, and with Ni-F8 the TON of the photocatalytic system was limited solely by decomposition of the ruthenium photosensitizer. This work represents a significant advance in the field of solar fuel since it provides a rare example of homogeneous light-driven water

oxidation catalyzed by Ni-based molecular catalyst, and this in neutral to acidic aqueous solutions. Last but not least, it provides a clear framework to design molecular catalysts for photocatalysis: the electron-richness of the catalytic center should be fine-tuned with appropriate substituents, to balance the driving forces of catalytic water oxidation vs. electron transfer from the catalyst to PS^+.

Acknowledgements

We are grateful for the support from China Scholarship Council (CSC) for a personal grant to C. Liu (No. 201706360150). We also acknowledge Prof. E. Bouwman and Dr. D.G.H. Hetterscheid for scientific discussion and support.

Conflict of interest

The authors declare no conflict of interest.

Keywords: homogeneous photocatalysis · molecular catalysts · nickel · porphyrins · water oxidation

[1] W. Zhang, W. Lai, R. Cao, *Chem. Rev.* **2017**, *117*, 3717 – 3797.
[2] D. K. Dogutan, D. G. Nocera, *Acc. Chem. Res.* **2019**, *52*, 3143 – 3148.
[3] B. Limburg, E. Bouwman, S. Bonnet, *Coord. Chem. Rev.* **2012**, *256*, 1451 – 1467.
[4] H.-C. Chen, D. G. H. Hetterscheid, R. M. Williams, J. I. van der Vlugt, J. N. H. Reek, A. M. Brouwer, *Energy Environ. Sci.* **2015**, *8*, 975 – 982.
[5] J. L. Fillol, Z. Codola, I. Garcia-Bosch, L. Gomez, J. J. Pla, M. Costas, *Nat. Chem.* **2011**, *3*, 807 – 813.
[6] M. D. Kärkäs, O. Verho, E. V. Johnston, B. Åkermark, *Chem. Rev.* **2014**, *114*, 11863 – 12001.
[7] T. J. Meyer, M. V. Sheridan, B. D. Sherman, *Chem. Soc. Rev.* **2017**, *46*, 6148 – 6169.
[8] L. Duan, F. Bozoglian, S. Mandal, B. Stewart, T. Privalov, A. Llobet, L. Sun, *Nat. Chem.* **2012**, *4*, 418 – 423.
[9] N. Vereshchuk, R. Matheu, J. Benet-Buchholz, M. Pipelier, J. Lebreton, D. Dubreuil, A. Tessier, C. Gimbert-Surinach, M. Z. Ertem, A. Llobet, *J. Am. Chem. Soc.* **2020**, *142*, 5068 – 5077.
[10] Z. Li, N. A. Leed, N. M. Dickson-Karn, K. R. Dunbar, C. Turro, *Chem. Sci.* **2014**, *5*, 727 – 737.
[11] S. Ye, C. Ding, M. Liu, A. Wang, Q. Huang, C. Li, *Adv. Mater.* **2019**, *31*, 1902069.
[12] S. Dey, T. K. Todorova, M. Fontecave, V. Mougel, *Angew. Chem. Int. Ed.* **2020**, *59*, 15726 – 15733; *Angew. Chem.* **2020**, *132*, 15856 – 15863.
[13] L. Duan, Y. Xu, P. Zhang, M. Wang, L. Sun, *Inorg. Chem.* **2010**, *49*, 209 – 215.
[14] N. Kaveevivitchai, R. Chitta, R. Zong, M. El Ojaimi, R. P. Thummel, *J. Am. Chem. Soc.* **2012**, *134*, 10721 – 10724.
[15] L. Tong, R. P. Thummel, *Chem. Sci.* **2016**, *7*, 6591 – 6603.
[16] D. J. Wasylenko, R. D. Palmer, C. P. Berlinguette, *Chem. Commun.* **2013**, *49*, 218 – 227.
[17] M. P. Santoni, G. La Ganga, V. Mollica Nardo, M. Natali, F. Puntoriero, F. Scandola, S. Campagna, *J. Am. Chem. Soc.* **2014**, *136*, 8189 – 8192.
[18] B. Schwarz, J. Forster, M. K. Goetz, D. Yucel, C. Berger, T. Jacob, C. Streb, *Angew. Chem. Int. Ed.* **2016**, *55*, 6329 – 6333; *Angew. Chem.* **2016**, *128*, 6437 – 6441.
[19] E. A. Karlsson, B. L. Lee, T. Akermark, E. V. Johnston, M. D. Karkas, J. Sun, O. Hansson, J. E. Backvall, B. Akermark, *Angew. Chem. Int. Ed.* **2011**, *50*, 11715 – 11718; *Angew. Chem.* **2011**, *123*, 11919 – 11922.
[20] C. Panda, J. Debgupta, D. Diaz Diaz, K. K. Singh, S. Sen Gupta, B. B. Dhar, *J. Am. Chem. Soc.* **2014**, *136*, 12273 – 12282.
[21] B. Das, A. Orthaber, S. Ott, A. Thapper, *ChemSusChem* **2016**, *9*, 1178 – 1186.
[22] Y. Zhao, J. Lin, Y. Liu, B. Ma, Y. Ding, M. Chen, *Chem. Commun.* **2015**, *51*, 17309 – 17312.
[23] T. Nakazono, A. R. Parent, K. Sakai, *Chem. Commun.* **2013**, *49*, 6325 – 6327.
[24] T. Nakazono, A. R. Parent, K. Sakai, *Chem. Eur. J.* **2015**, *21*, 6723 – 6726.
[25] T. Nakazono, K. Sakai, *Dalton Trans.* **2016**, *45*, 12649 – 12652.
[26] M. A. Asraf, H. A. Younus, C. I. Ezugwu, A. Mehta, F. Verpoort, *Catal. Sci. Technol.* **2016**, *6*, 4271 – 4282.
[27] E. Pizzolato, M. Natali, B. Posocco, A. Montellano Lopez, I. Bazzan, M. Di Valentin, P. Galloni, V. Conte, M. Bonchio, F. Scandola, A. Sartorel, *Chem. Commun.* **2013**, *49*, 9941 – 9943.
[28] T. Ishizuka, A. Watanabe, H. Kotani, D. Hong, K. Satonaka, T. Wada, Y. Shiota, K. Yoshizawa, K. Ohara, K. Yamaguchi, S. Kato, S. Fukuzumi, T. Kojima, *Inorg. Chem.* **2016**, *55*, 1154 – 1164.
[29] N. S. McCool, D. M. Robinson, J. E. Sheats, G. C. Dismukes, *J. Am. Chem. Soc.* **2011**, *133*, 11446 – 11449.
[30] F. Evangelisti, R. Guttinger, R. More, S. Luber, G. R. Patzke, *J. Am. Chem. Soc.* **2013**, *135*, 18734 – 18737.
[31] S. Berardi, G. La Ganga, M. Natali, I. Bazzan, F. Puntoriero, A. Sartorel, F. Scandola, S. Campagna, M. Bonchio, *J. Am. Chem. Soc.* **2012**, *134*, 11104 – 11107.
[32] F. Song, R. More, M. Schilling, G. Smolentsev, N. Azzaroli, T. Fox, S. Luber, G. R. Patzke, *J. Am. Chem. Soc.* **2017**, *139*, 14198 – 14208.
[33] C.-F. Leung, S.-M. Ng, C.-C. Ko, W.-L. Man, J. Wu, L. Chen, T.-C. Lau, *Energy Environ. Sci.* **2012**, *5*, 7903.
[34] H. Y. Wang, E. Mijangos, S. Ott, A. Thapper, *Angew. Chem. Int. Ed.* **2014**, *53*, 14499 – 14502; *Angew. Chem.* **2014**, *126*, 14727 – 14730.
[35] J. Lin, X. Meng, M. Zheng, B. Ma, Y. Ding, *Appl. Catal. B* **2019**, *241*, 351 – 358.
[36] R. Terao, T. Nakazono, A. R. Parent, K. Sakai, *ChemPlusChem* **2016**, *81*, 1064 – 1067.
[37] R. J. Xiang, H. Y. Wang, Z. J. Xin, C. B. Li, Y. X. Lu, X. W. Gao, H. M. Sun, R. Cao, *Chem. Eur. J.* **2016**, *22*, 1602 – 1607.
[38] M. Zhang, M. T. Zhang, C. Hou, Z. F. Ke, T. B. Lu, *Angew. Chem. Int. Ed.* **2014**, *53*, 13042 – 13048; *Angew. Chem.* **2014**, *126*, 13258 – 13264.
[39] Y. Han, Y. Wu, W. Lai, R. Cao, *Inorg. Chem.* **2015**, *54*, 5604 – 5613.
[40] J.-W. Wang, X.-Q. Zhang, H.-H. Huang, T.-B. Lu, *ChemCatChem* **2016**, *8*, 3287 – 3293.
[41] P. Garrido-Barros, S. Grau, S. Drouet, J. Benet-Buchholz, C. Gimbert-Suriñach, A. Llobet, *ACS Catal.* **2019**, *9*, 3936 – 3945.
[42] G. Chen, L. Chen, S. M. Ng, T. C. Lau, *ChemSusChem* **2014**, *7*, 127 – 134.
[43] L. Francàs, R. Matheu, E. Pastor, A. Reynal, S. Berardi, X. Sala, A. Llobet, J. R. Durrant, *ACS Catal.* **2017**, *7*, 5142 – 5150.
[44] U. S. Akhtar, E. L. Tae, Y. S. Chun, I. C. Hwang, K. B. Yoon, *ACS Catal.* **2016**, *6*, 8361 – 8369.
[45] W. C. Ellis, N. D. McDaniel, S. Bernhard, T. J. Collins, *J. Am. Chem. Soc.* **2010**, *132*, 10990 – 10991.
[46] B. Limburg, G. Laisne, E. Bouwman, S. Bonnet, *Chem. Eur. J.* **2014**, *20*, 8965 – 8972.

[47] L. Huang, Y. Chen, G. Y. Gao, X. P. Zhang, *J. Org. Chem.* **2003**, *68*, 8179 – 8184.
[48] M. F. Zipplies, W. A. Lee, T. C. Bruice, *J. Am. Chem. Soc.* **1986**, *108*, 4433 – 4445.
[49] S. Nakagaki, F. L. Benedito, F. Wypych, *J. Mol. Catal. A* **2004**, *217*, 121 – 131.
[50] J. C. Biffinger, H. Sun, A. P. Nelson, S. G. DiMagno, *Org. Biomol. Chem.* **2003**, *1*, 733 – 736.
[51] K. Bütje, K. Nakamoto, *Inorg. Chim. Acta* **1990**, *167*, 97 – 108.
[52] P. K. Ghosh, B. S. Brunschwig, M. Chou, C. Creutz, N. Sutin, *J. Am. Chem. Soc.* **1984**, *106*, 4772 – 4783.
[53] B. Limburg, E. Bouwman, S. Bonnet, *ACS Catal.* **2016**, *6*, 5273 – 5284.
[54] M. D. Kärkäs, B. Åkermark, *Dalton Trans.* **2016**, *45*, 14421 – 14461.
[55] X. Zhang, Y. Y. Li, J. Jiang, R. Zhang, R. Z. Liao, M. Wang, *Inorg. Chem.* **2020**, *59*, 5424 – 5432.

Manuscript received: March 3, 2021
Accepted manuscript online: March 26, 2021
Version of record online: May 3, 2021

